Comparison of the magnetic properties of isoelectronic $Sr_x(Na_{0.5}La_{0.5})_{1-x}RuO_3$ and $Sr_xCa_{1-x}RuO_3$ perovskites

T. He
Department of Chemistry and Princeton Materials Institute, Princeton University, Princeton, New Jersey 08540

Q. Huang
NIST Center for Neutron Research, National Institute of Standards and Technology, Gaithersburg, Maryland 20899 and Department of Materials and Nuclear Engineering, University of Maryland, College Park, Maryland 20742

R. J. Cava
Department of Chemistry and Princeton Materials Institute, Princeton University, Princeton, New Jersey 08540
(Received 17 July 2000; published 11 December 2000)

The solid solution $Sr_x(Na_{0.5}La_{0.5})_{1-x}RuO_3$ $(0 \leqslant x \leqslant 1)$ is reported, and its structural, electronic, and magnetic properties are compared to isoelectronic $Sr_xCa_{1-x}RuO_3$. The suppression of ferromagnetic interactions in $Sr_xCa_{1-x}RuO_3$ has frequently been attributed to the orthorhombic structural distortion, either through the crossover to classical antiferromagnetic interactions, or to a nearly ferromagnetic metal. Comparison of the magnetic properties of $Sr_x(Na_{0.5}La_{0.5})_{1-x}RuO_3$ to $Sr_xCa_{1-x}RuO_3$, however, shows that there is a much faster suppression of ferromagnetic interactions in the former case. Neither orthorhombic distortion nor cation size disorder can explain the observed difference. Instead, the difference may be attributed to charge disorder on the *A* site, which affects the local environment of Ru atoms greatly and leads to the faster suppression of the long-range ferromagnetic state.

DOI: 10.1103/PhysRevB.63.024402 PACS number(s): 75.30.Cr, 75.50.Cc, 61.12.Ld

I. INTRODUCTION

The perovskite-based ruthenates have been of great recent interest due to the coexistence of ferromagnetism and superconductivity in a single structural family. Three-dimensional $SrRuO_3$ is metallic, and ferromagnetic below $T_c \sim 160$ K.[1] Double-layer $Sr_3Ru_2O_7$ has a local moment at high temperatures and develops antiferromagnetic correlations below 15 K, but the spins do not order magnetically down to very low temperatures.[2,3] The single layer compound Sr_2RuO_4 displays no local Ru moment and is superconducting at about 1 K.[4]

The ferromagnetism of $SrRuO_3$ is at first unexpected, as according to expectations, the $t_{2g}(d^{4+})-O_{2p}-t_{2g}(d^{4+})$ type superexchange interaction in a perovskite structure should be antiferromagnetic.[5] The expected magnetic ground state for the ruthenate perovskites becomes even more problematic when $SrRuO_3$ is compared with the closely related compound $CaRuO_3$. Although they are isoelectronic and have similar orthorhombic unit cells, $CaRuO_3$ has a large negative Curie–Weiss temperature, -110 K, and shows no long range magnetic ordering. This has variously been attributed to the difference in size between Sr and Ca and the correspondingly greater lattice distortion in $CaRuO_3$,[1] the effect of *A* cations on the widths of the $4d$ bands and hence on the relative populations of the spin-up and spin-down bands,[6] or the greater Lewis acidity of Ca^{2+} compared to that of Sr^{2+}.[7] Band structure calculations have supported the importance of the structural distortion. In one such calculation, the density of states of $SrRuO_3$ was found to have a strong peak at the Fermi level, stabilizing ferromagnetism; while $CaRuO_3$ was found to be on the border of ferromagnetism and paramagnetism due to the fact that its more distorted structure lowered the density of states at the Fermi level.[8] In another calculation, ferromagnetic ground states were found for both compounds, but the calculated energies, especially for $CaRuO_3$, were very sensitive to calculational parameters.[9] It has also been argued that the larger structural distortion in $CaRuO_3$ would result in larger splitting of Ru t_{2g} orbitals, in turn, leading to stronger antiferromagnetic interactions.[10]

Recently, a new context for understanding $CaRuO_3$ has been proposed. It questioned the validity of regarding the Curie–Weiss (CW) behavior of $\chi(T)$ as the proof of the local moment nature and antiferromagnetic coupling of Ru spins.[11] Instead, it said that the change in magnetic properties of $Sr_xCa_{1-x}RuO_3$ could be explained quantitatively by the spin-fluctuation theory of itinerant-electron magnetism. On going from $SrRuO_3$ to $CaRuO_3$, the system changes from an intermediate itinerant ferromagnet, through weakly itinerant ferromagnet, to a nearly ferromagnetic metal. This viewpoint was supported by the measurements of specific heat and high-field magnetization,[12,13] and was further supported by Ru and ^{17}O NMR studies.[11,14] This picture is consistent with theoretical models based on electronic structure calculations.[8]

Several studies have appeared which probe the properties of $Sr_xCa_{1-x}RuO_3$ perovskites.[10–15,16] The variation in properties may now be basically understood in terms of the change in magnetic ground state as a function of Ru–O–Ru bond angle,[8] but there may be other influences as well. Consideration of the *A*-site atom size disorder may be important. It has, for example, been shown that at the same doping level and mean *A*-site cation radius, the T_c in superconducting copper oxides and the transition temperature T_m in manga-

nate ferromagnets both show a strong linear decrease with *A*-site disorder.[17,18]

To study the magnetism further, and to test the effect of disorder on the magnetic properties, a series of $Sr_x(Na_{0.5}La_{0.5})_{1-x}RuO_3$ perovskites is reported. The structure, electrical, and magnetic properties of $Sr_x(Na_{0.5}La_{0.5})_{1-x}RuO_3$ are compared to the isoelectronic $Sr_xCa_{1-x}RuO_3$ series. Since the cation sizes decrease in the order $Sr^{2+}(1.44\,Å) > Na^{+}(1.39\,Å) > La^{2+}(1.36\,Å) > Ca^{2+}(1.34\,Å)$, a smaller orthorhombic distortion and a smaller size disorder would be expected for $Sr_x(Na_{0.5}La_{0.5})_{1-x}RuO_3$ than for $Sr_xCa_{1-x}RuO_3$. Contrary to the expectation based on Ru–O–Ru bond angle, however, a much quicker suppression of ferromagnetism was found in $Sr_x(Na_{0.5}La_{0.5})_{1-x}RuO_3$. Both orthorhombic distortion and cation size disorder effects are considered, and neither can account for the observed changes in the magnetic properties. Instead, the effect of *A*-site charge disorder is introduced. This disorder is derived from random distribution of Sr^{2+}, Na^{+}, and La^{3+} on the *A*-sites. It gives a qualitative explanation for the observed changes. In $Sr_x(Na_{0.5}La_{0.5})_{1-x}RuO_3$, there is less size disorder but more *A*-site charge disorder. The magnetic properties of $SrRuO_3$ are shown to be more sensitive to *A*-site charge disorder than to structural distortion.

II. EXPERIMENT

Samples of $Sr_x(Na_{0.5}La_{0.5})_{1-x}RuO_3$ were prepared by conventional solid state reaction using $SrCO_3$(99.99%), Na_2CO_3(99.999%), dried La_2O_3(99.99%), and dried RuO_2(99.95%). The starting materials were mixed in stoichiometric proportion and heated at 500 °C for four hours in air. The powders were then heated at 1000 °C for two days and at 1100 °C for one day in air with intermediate grindings. Finally, the samples were pressed into pellets and annealed at 1100 °C for three hours. Similar conditions were used to prepare samples of $Sr_xCa_{1-x}RuO_3$.

Powder neutron diffraction data were collected at the NIST Center for Neutron Research using the BT-1 high-resolution powder diffractometer. A Cu (311) monochromator was employed to produce monochromatic neutron beams of wavelength 1.5401 Å. Collimators with horizontal divergences of 15′, 20′, and 7′ of arc full-width at half-maximum were used before and after the monochromator, and after the sample, respectively. The intensities were measured in steps of 0.05° in the 2θ range 3°–168°. Data were collected at room temperature and the structural parameters were refined using the program GSAS.[19]

Electrical resistivity was measured in the range of 5–400 K using a standard four-lead AC technique on polycrystalline sample bars about 1 mm×1 mm×5 mm in size. The magnetic properties were studied in a commercial apparatus from QD. Data were collected in the temperature range 5–300 K for $Sr_x(Na_{0.5}La_{0.5})_{1-x}RuO_3$ and $Sr_xCa_{1-x}RuO_3$ at 1T on field cooling and 5–400 K at 6 T on field cooling. Since the $Sr_xCa_{1-x}RuO_3$ magnetic data in the literature vary,[10–13,15,16] we synthesized and measured the whole series under our own conditions to allow direct comparison.

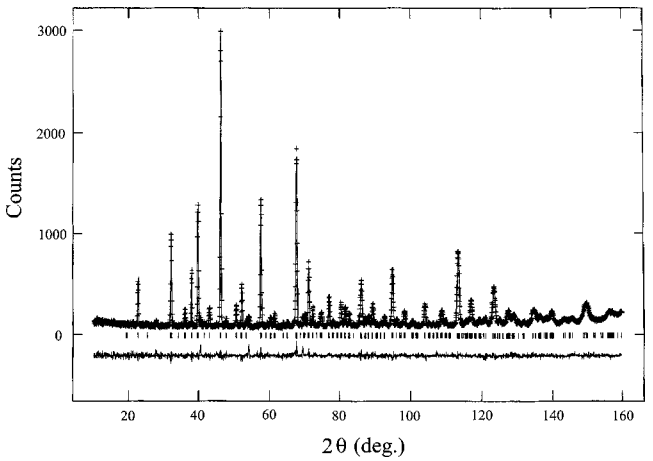

FIG. 1. Observed (+) and calculated (continuous line) powder neutron diffraction pattern for $Sr_{0.4}Na_{0.3}La_{0.3}RuO_3$ at 295 K. The difference curve between observed and calculated intensities is shown at the bottom of the figure.

III. RESULTS

Neutron diffraction data showed that all samples of $Sr_x(Na_{0.5}La_{0.5})_{1-x}RuO_3$ were single phase and had the $GdFeO_3$ type orthorhombic perovskite structure. Figure 1 shows the $x=0.4$ neutron diffraction pattern. Detailed results of the structural refinements are presented in Table I.[20] The cubic subcell parameters of $Sr_x(Na_{0.5}La_{0.5})_{1-x}RuO_3$ are shown in Fig. 2(a). All three lattice parameters decrease linearly when $Sr^{2+}(1.44\,Å)$ is substituted by smaller $La^{3+}(1.36\,Å)$ and $Na^{+}(1.39\,Å)$. There is, however, a change in the slope around $x=0.4$. The Ru–O–Ru bond angles show a discontinuity at this composition, as shown in Fig. 2(b). The rotation of RuO_6 octahedra changes character when *x* goes below 0.4, becoming more uniform, and is accompanied by a greater rate of decrease of the lattice parameters. Table II lists selected bond angles and bond distances for $Sr_x(Na_{0.5}La_{0.5})_{1-x}RuO_3$. There are no significant changes in the Ru–O bond lengths or the O–Ru–O bond angles within the RuO_6 octahedra across the series, consistent with former studies showing the rigidity of the RuO_6 octahedra in $Sr_xCa_{1-x}RuO_3$,[21] and as would be expected for solid solutions in which the Ru oxidation state is unchanged. Thus, the overall structural changes are in the Ru–O–Ru bond angle between octahedra, as shown in Fig. 2.

The temperature dependence of the resistivity for polycrystalline pellets of $Sr_x(Na_{0.5}La_{0.5})_{1-x}RuO_3$ is shown in Fig. 3. $SrRuO_3$ is metallic with the expected kink in the resistivity curve at the ferromagnetic transition temperature 160 K. On (La/Na) doping, the resistivity increases systematically, but remains metallic for the whole series. In contrast, the resistivity in $Sr_xCa_{1-x}RuO_3$ charges little in the paramagnetic temperature range, and there is no clear trend at low temperatures.[10] The $Sr_xCa_{1-x}RuO_3$ data show that the orthorhombic distortion has no big effect on the observed resistivity. We attribute the increasing resistivity in $Sr_x(Na_{0.5}La_{0.5})_{1-x}RuO_3$ to be due to the effect of *A*-site charge disorder, described in detail with regard to the magnetic properties. The different charges on the *A*-site cations

TABLE I. Structural parameters for $ARuO_3$ at 295 K. $A=Sr_x(La_{0.5}Na_{0.5})_{1-x}$. Space group: *Pnma* (#62). Atomic positions: A(La/Na/Sr): $4c(x,1/4,z)$; Ru: $4b(0,0,1/2)$; O(1): $4c(x,1/4,z)$; O(2) $8d(x,y,z)$.

	$(x=)$	0	0.1	0.2	0.3	0.4	0.5	0.6	0.7	0.8	0.9	1.0
	a (Å)	5.5001(3)	5.5058(3)	5.5099(3)	5.5145(3)	5.5202(3)	5.5220(2)	5.5230(3)	5.5263(3)	5.5287(3)	5.5312(3)	5.5320(2)
	b (Å)	7.7857(4)	7.7943(5)	7.8008(4)	7.8098(4)	7.8186(3)	7.8207(3)	7.8258(4)	7.8306(4)	7.8369(4)	7.8444(4)	7.8463(3)
	c (Å)	5.5087(3)	5.5168(3)	5.5227(4)	5.5312(3)	5.5406(3)	5.5463(2)	5.5512(3)	5.5572(3)	5.5620(3)	5.5673(3)	5.5684(2)
	V (Å^3)	235.89(2)	236.75(2)	237.37(2)	238.21(2)	239.13(2)	239.52(2)	239.93(3)	240.49(3)	240.99(3)	241.56(3)	241.70(2)
A	x	0.0253(6)	0.0246(5)	0.0215(6)	0.0217(6)	0.0197(5)	0.0194(5)	0.0182(7)	0.0184(7)	0.0183(6)	0.0176(6)	0.0166(5)
	z	−0.008(1)	−0.005(1)	−0.007(1)	−0.004(1)	−0.003(1)	−0.0067(7)	−0.0077(9)	−0.0046(9)	−0.0046(8)	−0.0029(8)	−0.0034(6)
	U (Å^2)	0.0103(5)	0.0100(5)	0.0106(5)	0.0107(5)	0.0108(4)	0.0103(4)	0.0086(5)	0.0092(5)	0.0087(4)	0.0079(5)	0.0089(4)
Ru	U (Å^2)	0.0094(3)	0.0091(3)	0.0089(4)	0.0084(4)	0.0094(4)	0.0093(3)	0.0096(5)	0.0095(4)	0.0089(4)	0.0074(4)	0.0068(3)
O(1)	x	0.4902(7)	0.4890(7)	0.4918(8)	0.4925(9)	0.4920(8)	0.4933(7)	0.4950(9)	0.4953(9)	0.4945(8)	0.4953(9)	0.4973(7)
	z	0.073(1)	0.072(1)	0.067(1)	0.066(1)	0.058(1)	0.0566(8)	0.057(1)	0.0563(9)	0.0541(8)	0.0532(8)	0.0524(6)
	U_{11} (Å^2)	0.018(3)	0.018(3)	0.021(3)	0.024(4)	0.019(3)	0.012(2)	0.008(2)	0.012(2)	0.014(2)	0.018(2)	0.014(2)
	U_{22} (Å^2)	0.002(2)	0.012(2)	0.000(2)	0.000(2)	0.000(2)	0.005(2)	0.000(2)	0.000(2)	0.000(2)	0.003(2)	0.000(2)
	U_{33} (Å^2)	0.020(3)	0.013(3)	0.035(3)	0.029(3)	0.027(2)	0.026(2)	0.029(2)	0.024(2)	0.023(2)	0.013(2)	0.017(1)
	U_{13} (Å^2)	0.006(1)	0.006(1)	0.005(2)	0.008(2)	0.002(2)	0.006(2)	0.007(2)	0.000(2)	−0.000(2)	−0.004(2)	−0.005(2)
O(2)	x	0.2874(5)	0.2872(5)	0.2859(5)	0.2847(5)	0.2845(4)	0.2841(4)	0.2835(5)	0.2813(5)	0.2806(5)	0.2776(5)	0.2775(4)
	y	0.0390(6)	0.0372(6)	0.0370(5)	0.0355(5)	0.0364(4)	0.0343(4)	0.0326(5)	0.0317(4)	0.0302(4)	0.0288(4)	0.0276(3)
	z	0.7146(6)	0.7168(5)	0.7175(6)	0.7187(5)	0.7191(5)	0.7208(4)	0.7209(6)	0.7232(5)	0.7231(5)	0.7240(4)	0.7233(4)
	U_{11} (Å^2)	0.012(1)	0.010(1)	0.013(1)	0.011(1)	0.0010(9)	0.0107(8)	0.012(1)	0.012(1)	0.014(1)	0.012(1)	0.0109(8)
	U_{22} (Å^2)	0.022(2)	0.020(2)	0.016(1)	0.017(2)	0.018(1)	0.022(1)	0.022(2)	0.021(2)	0.018(1)	0.017(1)	0.014(1)
	U_{33} (Å^2)	0.012(2)	0.012(1)	0.012(1)	0.011(1)	0.014(1)	0.0138(9)	0.012(1)	0.010(1)	0.010(1)	0.007(1)	0.0096(8)
	U_{12} (Å^2)	−0.005(1)	−0.004(1)	−0.007(1)	−0.004(1)	−0.0060(9)	−0.0064(9)	−0.005(1)	−0.006(1)	−0.004(1)	−0.004(1)	−0.0034(9)
	U_{13} (Å^2)	−0.005(1)	−0.009(1)	−0.003(1)	−0.004(1)	−0.005(1)	−0.007(1)	−0.004(1)	−0.004(1)	−0.005(1)	−0.004(1)	−0.002(1)
	U_{23} (Å^2)	0.007(2)	0.005(2)	0.009(1)	0.006(1)	0.003(1)	0.007(1)	0.008(1)	0.004(1)	0.0029(1)	0.001(1)	0.000(1)
	R_p(%)	4.94	4.67	6.04	5.22	5.29	4.95	6.74	6.39	6.10	6.47	6.02
	R_{wp}(%)	6.35	5.87	7.48	7.41	7.16	6.50	8.60	8.21	7.88	8.29	7.62
	χ^2	1.122	1.029	1.398	1.701	1.376	1.192	0.9379	0.9408	0.9157	0.9215	0.8601

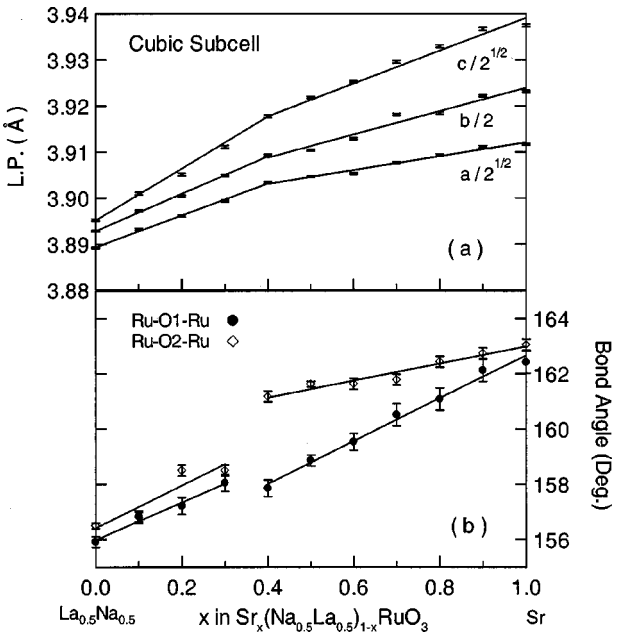

FIG. 2. Selected structural data for $Sr_x(Na_{0.5}La_{0.5})_{1-x}RuO_3$. Figure 2(a) shows the cubic subcell parameters of $Sr_x(Na_{0.5}La_{0.5})_{1-x}RuO_3$, and Fig. 2(b) shows the Ru–O(1)–Ru (●) and Ru–O(2)–Ru (◇) bond angles. Lines are guides to the eye.

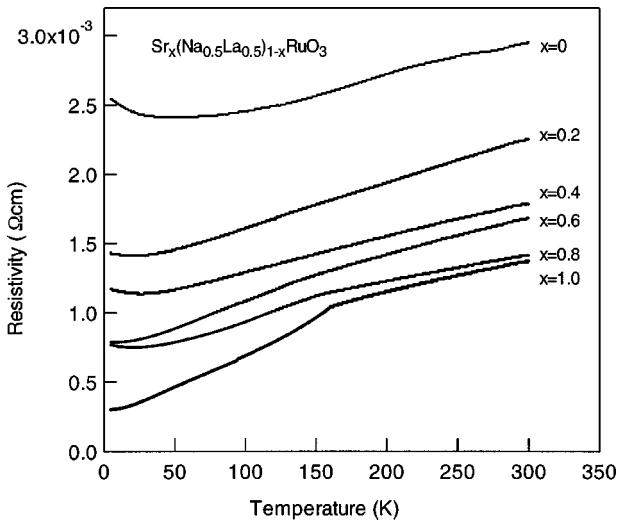

FIG. 3. Temperature dependence of the electrical resistivity of polycrystalline samples of $Sr_x(Na_{0.5}La_{0.5})_{1-x}RuO_3$.

can affect the local environment of Ru atoms greatly, and cause variations in the electron densities in the Ru–O network, which are effective in scattering electrons.

The magnetic properties of the perovskite series are more complex. The temperature dependence of inverse magnetic susceptibility measured at 1T on field cooling for both series is displayed in Fig. 4. It can be seen that both series are well described by the Curie–Weiss law at high temperatures, while there are broad downward drops in $1/\chi$ in intermediate temperature regimes in samples with mixed *A* cations. This phenomenon was observed previously for $Sr_xCa_{1-x}RuO_3$ and was attributed to the occurrence of Sr^{2+} clusters in the solid solution, leading to short-range ordered regions of $SrRuO_3$.[15] The downward drops in $1/\chi$ disappear when the magnetic field is increased from 1 T to 6 T. This shows that magnetic interactions in these compounds have some field dependence.

Figure 5 shows the effective magnetic moment $\mu_{\rm eff}$ and the Curie–Weiss temperature, $\theta_{\rm CW}$, as a function of composition for $Sr_x(Na_{0.5}La_{0.5})_{1-x}RuO_3$ and $Sr_xCa_{1-x}RuO_3$, derived from the data in Fig. 4. The effective magnetic moments in $Sr_xCa_{1-x}RuO_3$ decrease smoothly with composition from 2.7 to 2.1 μ_B/Ru. For the (La/Na) doped series, the moments decrease from 2.7 μ_B/Ru to 2.3 μ_B/Ru at intermediate composition and then increase back to 2.7 μ_B/Ru. The increase in effective Ru moment occurs at the same composition as the structural distortion between $x=0.3$ and 0.4. Subtle structural distortions or discontinuities in perovskites,

TABLE II. Selected interatomic distances (Å) and angles (°) for $ARuO_3$ at 295 K. $A=Su_x(La_{0.5}Na_{0.5})_{1-x}$.

	(*x*=)	0.0	0.1	0.2	0.3	0.4	0.5	0.6	0.7	0.8	0.9	1.0
A-O(1)	×1	2.976(5)	2.980(5)	2.947(6)	2.944(6)	2.932(5)	2.926(4)	2.912(6)	2.911(6)	2.914(5)	2.906(6)	2.890(5)
−O(1)	×1	2.596(5)	2.592(5)	2.623(6)	2.625(6)	2.629(5)	2.641(4)	2.658(6)	2.657(6)	2.653(5)	2.661(1)	2.677(5)
−O(1)	×1	3.117(9)	3.130(8)	3.095(9)	3.116(9)	3.079(7)	3.054(5)	3.051(7)	3.068(6)	3.060(6)	3.067(6)	3.059(5)
−O(1)	×1	2.405(9)	2.401(8)	2.438(9)	2.425(9)	2.471(7)	2.500(5)	2.506(7)	2.495(6)	2.509(6)	2.506(6)	2.513(5)
A-O(2)	×2	2.667(4)	2.681(4)	2.683(4)	2.695(5)	2.701(4)	2.696(4)	2.704(5)	2.706(5)	2.714(4)	2.719(4)	2.728(3)
−O(2)	×2	2.761(5)	2.755(5)	2.771(5)	2.762(5)	2.775(4)	2.777(4)	2.775(5)	2.774(4)	2.768(4)	2.768(4)	2.763(3)
−O(2)	×2	3.260(4)	3.239(4)	3.231(4)	3.212(4)	3.211(4)	3.204(3)	3.194(4)	3.171(4)	3.163(3)	3.140(3)	3.134(3)
−O(2)	×2	2.389(5)	2.413(5)	2.408(5)	2.434(5)	2.431(4)	2.438(3)	2.445(4)	2.473(4)	2.484(4)	2.508(4)	2.509(3)
Ru–O(1)	×2	1.988(2)	1.989(1)	1.985(1)	1.987(1)	1.9814(9)	1.9806(7)	1.9819(9)	1.9827(8)	1.9825(7)	1.9835(6)	1.9832(5)
Ru–O(2)	×2	1.983(4)	1.974(3)	1.977(4)	1.977(3)	1.979(3)	1.972(2)	1.974(3)	1.972(3)	1.974(3)	1.982(2)	1.984(2)
−O(2)	×2	1.997(4)	2.004(3)	2.002(3)	2.001(3)	2.005(3)	2.008(2)	2.005(3)	2.004(3)	2.001(2)	1.991(2)	1.987(2)
Avg. Ru–O		1.989	1.989	1.988	1.988	1.988	1.987	1.987	1.986	1.986	1.986	1.985
Ru–O(1)–Ru		156.5(4)	156.8(4)	158.5(4)	158.5(4)	161.2(3)	161.6(2)	161.6(3)	161.8(3)	162.4(3)	162.7(2)	163.1(2)
Ru–O(2)–Ru		155.9(2)	156.9(2)	157.2(2)	158.1(2)	157.9(2)	158.9(1)	159.5(2)	160.5(2)	161.1(2)	161.1(2)	162.4(1)

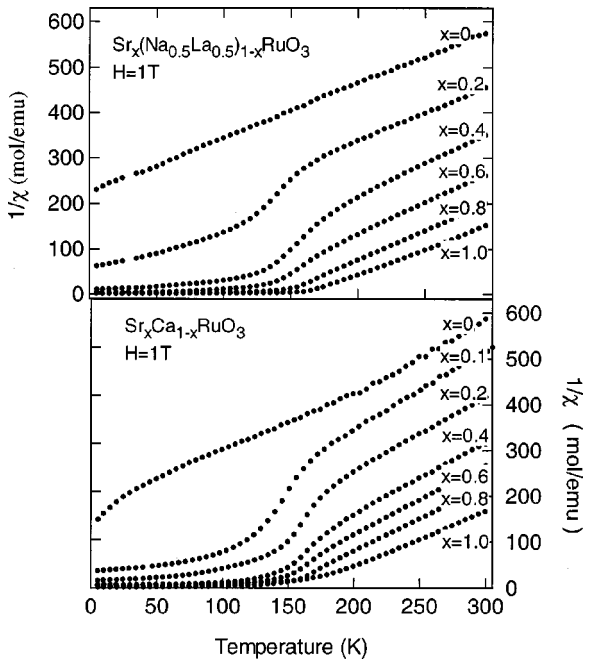

FIG. 4. Temperature dependence of the inverse magnetic susceptibility measured at 1 T on field cooling for $Sr_x(Na_{0.5}La_{0.5})_{1-x}RuO_3$ and Sr_xCaRuO_3.

such as those seen here, can often be an indicator of delicate electron/lattice interactions.[22] Further detailed study of this composition region may be of interest. All samples show Curie–Weiss-like behavior in the high temperature regimes. The θ_{CW}'s are fit in the temperature range of 175–300 K. A

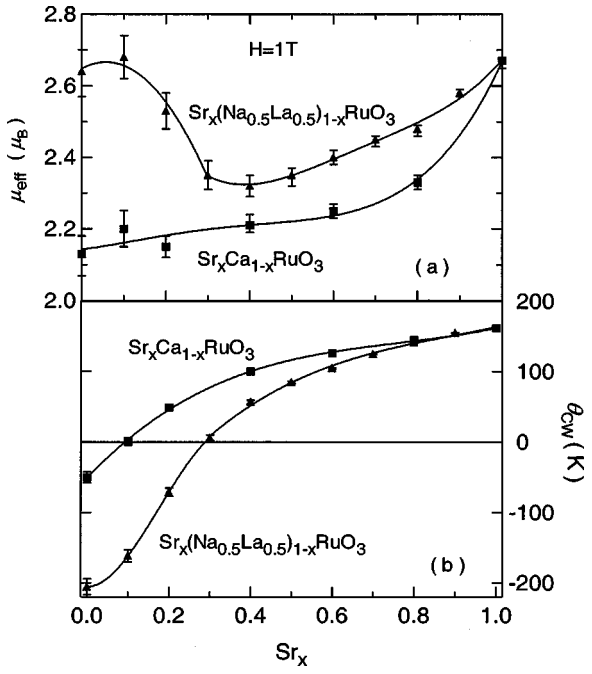

FIG. 5. Component dependence of (a) the effective magnetic moment and (b) Curie–Weiss temperatures for $Sr_x(Na_{0.5}La_{0.5})_{1-x}RuO_3$ (▲) and Sr_xCaRuO_3 (■). Lines are guides to the eye.

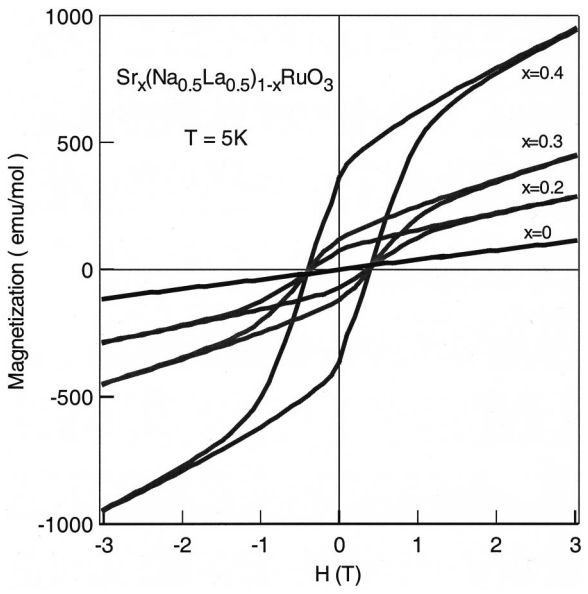

FIG. 6. Magnetic hysterisis loops for $Sr_x(Na_{0.5}La_{0.5})_{1-x}RuO_3$ at 5 K with $x=0.4$, 0.3, 0.2, and 0, respectively.

temperature independent term, χ_0, was determined to a precision of $\pm 5\times 10^{-5}$ emu/mol Ru and is included in the fits. The Curie–Weiss temperatures decrease smoothly with composition in both series. This is consistent with previous studies of $Sr_xCa_{1-x}RuO_3$, and has been interpreted as being due to the effect of orthorhombic distortion on the magnetic properties. If distortion were the dominant factor in suppressing ferromagnetic interactions, then a lower θ_{CW} would be expected in $Sr_xCa_{1-x}RuO_3$ than in $Sr_x(Na_{0.5}La_{0.5})_{1-x}RuO_3$ at the same doping level due to the smaller size of Ca^{2+} compared to $(Na_{0.5}La_{0.5})^{2+}$, and the larger resulting structural distortion. The present experiments, however, show the opposite results: there is a much faster suppression of θ_{CW} in $Sr_x(Na_{0.5}La_{0.5})_{1-x}RuO_3$ than in $Sr_xCa_{1-x}RuO_3$. This can be seen, for example, by the fact that the transformation from positive to negative θ_{CW} happens at a lower doping level in $Sr_x(Na_{0.5}La_{0.5})_{1-x}RuO_3$. This suggests that although the distortion may be effective in suppressing ferromagnetic interactions, it may not be the only significant factor.

The θ_{CW}'s in (La/Na) doped samples change from positive to negative when x is close to 0.3. Ferromagnetism is still present, however, for samples with $\theta_{CW}<0$. The compound $Sr_{0.2}(Na_{0.5}La_{0.5})_{0.8}RuO_3$, for example, shows a magnetic hysteresis loop even with a negative θ_{CW}. Figure 6 shows the hysteresis loops measured at 5 K for $Sr_x(Na_{0.5}La_{0.5})_{1-x}RuO_3$ with $x=0.4$, 0.3, 0.2, and 0, respectively. There are small ferromagnetic components to the magnetization at low temperatures for all values of x, except for the $x=0$ end member. The 6T measurement of magnetization is at sufficiently high field to be above the hysteresis loop for all compositions at all temperatures, and we therefore employ 6 T magnetization to parametrize the ferromagnetic moment. The temperature dependence of magnetization measured at 6 T on field cooling for both series is displayed in Fig. 7.

For a more detailed comparison, Fig. 8(a) shows θ_{CW} vs.

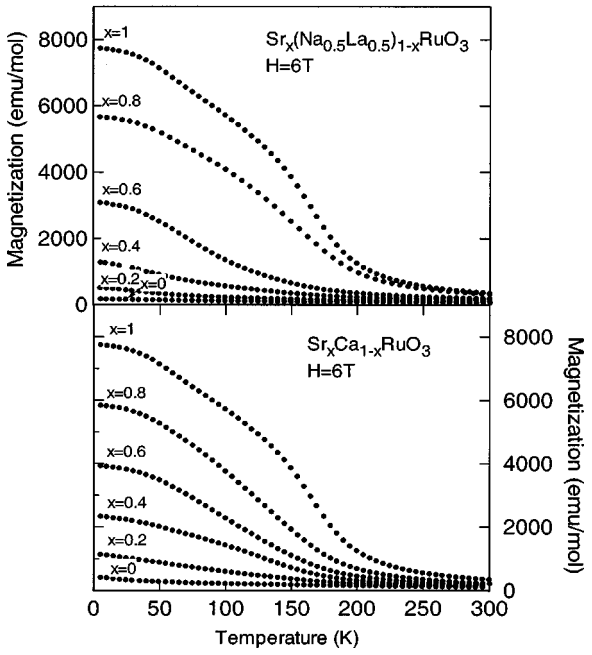

FIG. 7. Temperature dependence of magnetization measured at 6 T on field cooling for $Sr_x(Na_{0.5}La_{0.5})_{1-x}RuO_3$ and Sr_xCaRuO_3.

the average Ru–O–Ru intraoctahedra bond angle for both series, using the structural data from Fig. 2 for $Sr_x(Na_{0.5}La_{0.5})_{1-x}RuO_3$ and published structural data for $Sr_xCa_{1-x}RuO_3$.[20] The Ru–O–Ru bond angles are an indicator of the degree of orthorhombic distortion, and are the primary influence on the different electronic/magnetic states of

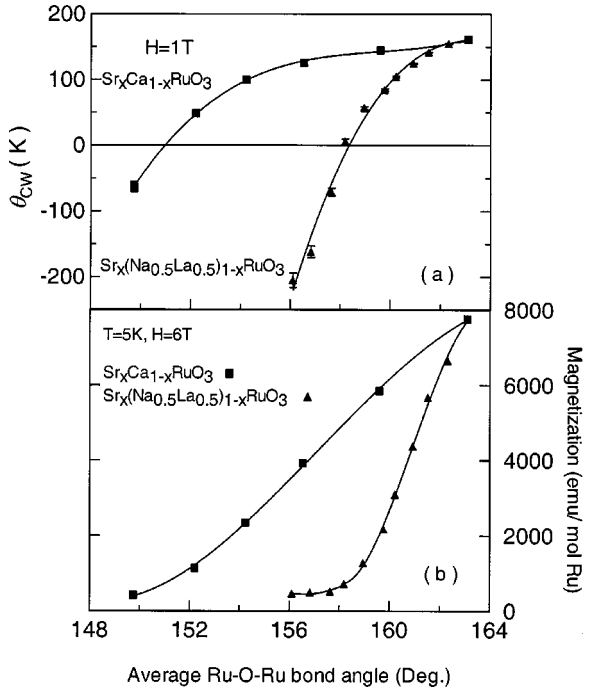

FIG. 8. (a) Curie–Weiss temperature ($H=1$ T) and (b) magnetization measured at 5 K in a field of 6T vs. the average Ru–O–Ru bond angle for $Sr_x(Na_{0.5}La_{0.5})_{1-x}RuO_3$ (▲) and Sr_xCaRuO_3 (■). Lines are guides to the eye.

$SrRuO_3$ and $CaRuO_3$. At any particular bond angle, i.e., if the degree of orthorhombic distortion is kept fixed, the (La/Na) doped sample has a lower θ_{CW} than the Ca-doped sample. This clearly shows that orthorhombic distortion cannot explain the differences in magnetic properties of these two series and cannot be the sole factor in suppressing ferromagnetic interactions. Figure 8(b) shows the magnetization at 5 K measured at 6 T for all samples in the two series, plotted as a function of the structural distortion via the Ru–O–Ru bond angle. The dramatic suppression of ferromagnetism for $Sr_x(Na_{0.5}La_{0.5})_{1-x}RuO_3$ can be seen.

IV. DISCUSSION

Structural distortions in perovskites which change the intraoctahedron M–O–M bond angle are expected to affect the electronic bandwidth. There have been intensive studies on the 3d-based perovskites with unpaired electrons in e_g orbitals. For the $L_{1-x}A_xMnO_3$ (L=RE,A=Ca, Sr) system, the $\sigma(e_g)$ bandwidth was found to have a $W(\theta)\approx\cos^2\theta$ dependence, where θ is the Mn–O–Mn bond angle.[23] Studies of the rare earth orthoferrites show that the Neel temperature, T_N, and $\cos^2\theta$ are linearly related.[24] The same relationship was found in the $REMe_{0.5}Mn_{0.5}O_3$ (Me=Ni, Co) system for T_c when $\theta\geqslant 140°$.[25]

There has been, however, little work on the 4d-based perovskites with unpaired electrons in t_{2g} orbitals. To get a more precise description about the relationship between θ_{CW} and bond angle for the ruthenate perovskites, calculations on the magnetic exchange interactions for t_{2g} compounds are needed. Experimental and theoretical studies of the 3d perovskites with unpaired electrons in e_g orbitals found that the magnetic interactions change from antiferromagnetic to ferromagnetic as the metal–oxygen–metal bond angle varies from 180° to 90°. The situation is more complex when the interacting orbitals are $t_{2g}-O_{2p}-t_{2g}$ as in the present system. As the bond angle decreases, the 180° π-type $p-d$ interaction decreases, but the σ-type-like $p-d$ interaction becomes stronger. Furthermore, interaction between two t_{2g} orbitals becomes possible. Detailed theoretical modeling of this system would be of significant interest.

It has recently been shown that at the same doping level and mean A-site cation radius $\langle r_A\rangle$, T_c in the cuprate superconductors and the ferromagnetic transition temperature T_c in manganate ferromagnets both decrease linearly with A-site disorder, parametrized by the variance in radii $\sigma^2=\langle r_A^2\rangle-\langle r_A\rangle^2$.[15,16] In the two series under study here, cation size disorder may also have a significant effect on the magnetic properties. Table III shows the calculated mean A-site cation radius, $\langle r_A\rangle$, and the size variance, σ^2, for both series. Although $\langle r_A\rangle$ is not fixed in the present study, the cation size disorder effect cannot account for the differences in the rate at which Ca substitution and (La/Na) substitution suppress the T_c of $SrRuO_3$. First, at equal x, $Sr_x(Na_{0.5}La_{0.5})_{1-x}RuO_3$ has a smaller σ^2 than $Sr_xCa_{1-x}RuO_3$ due to Sr^{2+} being closer in size to La^{3+} and Na^+ than to Ca^{2+}. Thus, if θ_{CW} were to decrease with σ^2, again $Sr_x(Na_{0.5}La_{0.5})_{1-x}RuO_3$ would have higher θ_{CW} values than $Sr_xCa_{1-x}RuO_3$. Second,

TABLE III. Statistical variance σ^2 (size disorder) in the distribution of $\underline{A}$-site radii $\sigma^2=\langle r_A^2\rangle-\langle r_A\rangle^2$.

	$\langle r_A\rangle$	σ^2		$\langle r_A\rangle$	σ^2
$SrRuO_3$	1.44	0	$SrRuO_3$	1.44	0
$Sr_{0.8}Ca_{0.2}$	1.42	0.0016	$Sr_{0.8}La_{0.1}Na_{0.1}$	1.427	0.0007
$Sr_{0.6}Ca_{0.4}$	1.40	0.0024	$Sr_{0.6}La_{0.2}Na_{0.2}$	1.414	0.0011
$Sr_{0.4}Ca_{0.6}$	1.38	0.0024	$Sr_{0.4}La_{0.3}Na_{0.3}$	1.401	0.001 15
$Sr_{0.2}Ca_{0.8}$	1.36	0.0016	$Sr_{0.2}La_{0.4}Na_{0.4}$	1.388	0.0009
$CaRuO_3$	1.34	0	$La_{0.5}Na_{0.5}RuO_3$	1.375	0.0002

σ^2 peaks at the intermediate doping levels in both series, while their θ_{CW}'s decease monotonically as Sr content decreases.

Since neither orthorhombic distortion nor cation size disorder can explain the much faster suppression of ferromagnetic interactions in $Sr_x(Na_{0.5}La_{0.5})_{1-x}RuO_3$, there must be other factors. One additional important factor may be charge disorder on the A site of $Sr_x(Na_{0.5}La_{0.5})_{1-x}RuO_3$, which can be parametrized in an analogous way as size disorder, i.e., $\sigma_{CD}^2=\langle Z_A^2\rangle-\langle Z_A\rangle^2$, where Z_A is the charge of A cation. There is no charge disorder in $Sr_xCa_{1-x}RuO_3$ because Sr and Ca are both divalent. In $Sr_x(Na_{0.5}La_{0.5})_{1-x}RuO_3$, however, single valent Na^+, divalent Sr^{2+}, and trivalent La^{3+} are disordered on the perovskite ''A'' site. Thus, locally, the $Ru^{IV}O_6$ octahedra surrounded by La^{3+} ions would behave more like $Ru^{III}O_6$ octahedra, whereas those surrounded by Na^+ ions would behave more like $Ru^{V}O_6$ octahedra. ($LaRu^{III}O_3$) is paramagnetic, and studies of $Sr_xLa_{1-x}RuO_3$ show that La^{3+} was more effective than Ca^{2+} in suppressing ferromagnetic interactions.[7] Sodium ruthenates do not form perovskite structures, and little is known about their magnetic properties. By introducing charge disorder, the local environment of ruthenium ions and their local charge state is greatly changed, and there must be fluctuations in the local electron densities throughout the ruthenium–oxygen network. These fluctuations change the ruthenium–oxygen hybridization and the interaction between ruthenium spins, and ferromagnetism is suppressed dramatically. Although there are no previously documented cases of this behavior, the present system appears to be a good example. In terms of the band structure picture, the La–Na–Sr charge disorder is expected to smear the peak in the density of states which is responsible for the ferromagnetism, and therefore suppress the ferromagnetism more for any particular amount of structural distortion. The decrease in θ_{CW} due to the structural distortion effect can be calculated by subtracting the θ_{CW} of the $Sr_xCa_{1-x}RuO_3$ solid solution from that of $SrRuO_3$, and the decrease in θ_{CW} due to the charge disorder effect can be calculated by subtracting the θ_{CW} of $Sr_x(Na_{0.5}La_{0.5})_{1-x}RuO_3$ from that of $Sr_xCa_{1-x}RuO_3$ at a particular Ru–O–Ru bond angle. Figure 9(a) compares these two effects on θ_{CW}. It is seen that charge disorder acts more strongly than structural distortion in decreasing θ_{CW}. Figure 9(b) compares the suppression of the 5 K magnetization of $SrRuO_3$ at 6 T due to these two effects. A similar conclusion can be drawn. The decrease in θ_{CW} and 5 K magnetization due to charge disorder are shown as a function of the variance in the charge disorder (σ_{CD}^2) in $Sr_x(Na_{0.5}La_{0.5})_{1-x}RuO_3$ in the inset. The low temperature magnetization is seen to be more immediately sensitive to charge disorder than is θ_{CW}.

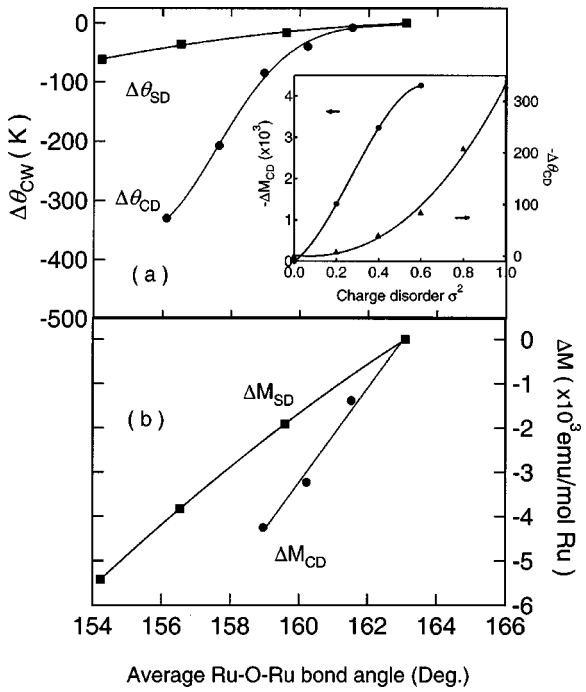

FIG. 9. Comparison of decrease in (a) Curie–Weiss temperatures, and (b) magnetization due to structural distortion (SD ■) and charge disorder (CD ●) effects. Lines are guides to the eye. Inset: Suppression of θ_{CW} (▲) and magnetization (●) due to charge disorder effect vs. charge disorder in $Sr_x(Na_{0.5}La_{0.5})_{1-x}RuO_3$.

One common feature of $Sr_x(Na_{0.5}La_{0.5})_{1-x}RuO_3$ and $Sr_xCa_{1-x}RuO_3$ is that their θ_{CW}'s decrease smoothly with doping. There have been two separate explanations for the smooth evolution of θ_{CW} from positive to negative in $Sr_xCa_{1-x}RuO_3$. The older explanation is based on the Curie–Weiss law, i.e., that positive θ_{CW} indicates ferromagnetic interactions and negative θ_{CW} indicates antiferromagnetic interactions between spins. In this scenario, both ferromagnetic and antiferromagnetic interactions are present in these compounds, and their ratio changes on going from $SrRuO_3$ to $CaRuO_3$. The strong Ru–O hybridization, which is found in $SrRuO_3$, stabilizes the ferromagnetic ground state. As Ca doping content increases, the Ru–O hybridization decreases and the spins become more localized. The $t_{2g}(d^{4+})-O_{2p}-t_{2g}(d^{4+})$ type superexchange interaction in a localized-electron system is expected to be antiferromagnetic. A continuous change of θ_{CW} in $Sr_xCa_{1-x}RuO_3$ could mean a continuous change in the relative strength of these two kinds of interactions. Recently, the validity of regarding the sign of the Curie–Weiss θ observed for $\chi(T)$ as an indication of the sign of the spin coupling has been called into question.[11] Instead, it said that the change in magnetic properties of $Sr_xCa_{1-x}RuO_3$ could be explained quantitatively by the spin-fluctuation theory of itinerant-electron magnetism. In this picture, consistent with one interpretation of the electronic structure calculations,[8] $CaRuO_3$ is poised at a quantum

critical boundary between ferromagnetism and paramagnetism. In both contexts, θ_{CW} is an order parameter which is a measure of how far the compounds proceed from an intermediate itinerant ferromagnet ($SrRuO_3$), through weakly itinerant ferromagnet, to an exotic nearly ferromagnetic metal ($CaRuO_3$).

$Sr_xCa_{1-x}RuO_3$ has attracted much attention due to its unusual and unexpected magnetic properties. Most former studies attributed the suppression of ferromagnetic interactions on substituting Sr^{2+} for Ca^{2+} to the orthorhombic structural distortion, either through the crossover to classical antiferromagnetic interactions, or to a nearly ferromagnetic metallic state. Here we have shown that comparison of the magnetic properties of $Sr_x(Na_{0.5}La_{0.5})_{1-x}RuO_3$ to $Sr_xCa_{1-x}RuO_3$ indicates that there is a much faster suppression of ferromagnetic interactions, observed in θ_{CW} and the low temperature magnetization for $Sr_x(Na_{0.5}La_{0.5})_{1-x}RuO_3$. Neither orthorhombic distortion nor cation size disorder can explain this dramatic change. Instead, we suggest that it is due to charge disorder on the *A*-site, which affects the local environment of Ru atoms greatly, leading to the faster suppression of the long-range ferromagnetic state. This appears to be the first example of off-site charge-disorder induced suppression of ferromagnetism observed for transition metal oxides.

ACKNOWLEDGMENTS

This work was supported by the National Science Foundation Grant No. DMR-9725979. We would like to acknowledge helpful conversations with A. Millis.

[1] A. Callaghan, C. W. Moeller, and R. Ward, Inorg. Chem. **5**, 1572 (1966).
[2] R. J. Cava, H. W. Zandbergen, J. J. Krajewski, W. F. Peck, Jr., B. Batlogg, S. Carter, R. M. Flemming, O. Zhou, and L. W. Rupp, Jr., Solid State Chem. **116**, 141 (1995).
[3] S.-I. Ikeda and Y. Maeno, Physica B **261**, 947 (1999).
[4] Y. Maeno, H. Hashimoto, K. Yoshida, S. Nishizaki, T. Fujita, J. G. Bednorz, and F. Lichtenberg, Nature (London) **372**, 532 (1994).
[5] J. B. Goodenough, *Magnetism and the Chemical Bond* (Interscience, New York, 1963).
[6] J. M. Longo, P. M. Raccah, and J. B. Goodenough, J. Appl. Phys. **39**, 1327 (1968).
[7] M. C. Fernanda, R. Greatrex, and N. N. Greenwood, Solid State Chem. **20**, 381 (1977).
[8] I. Mazin and D. J. Singh, Phys. Rev. B **56**, 2556 (1997).
[9] G. Santi and T. Jarlborg, J. Phys.: Condens. Matter **9**, 9563 (1997).
[10] F. Fukunaga and N. Tsuda, J. Phys. Soc. Jpn. **63**, 3798 (1994).
[11] K. Yoshimura, T. Imai, T. Kiyama, K. R. Thurber, A. W. Hunt, and K. Kosuge, Phys. Rev. Lett. **83**, 4397 (1999).
[12] T. Kiyama, K. Yoshimura, K. Kosuge, H. Michor, and G. Hilscher, J. Phys. Soc. Jpn. **67**, 307 (1998).
[13] T. Kiyama, K. Yoshimura, and K. Kosuge, J. Phys. Soc. Jpn. **68**, 3372 (1999).
[14] H. Mukuda, K. Ishida, Y. Kitaoka, K. Asayama, R. Kanno, and M. Takano, Phys. Rev. B **60**, 12 279 (1999).
[15] A. Kanbayasi, J. Phys. Soc. Jpn. **44**, 108 (1978).
[16] G. Cao, S. McCall, M. Shepard, and J. E. Crow, Phys. Rev. B **56**, 321 (1997).
[17] J. P. Attfield, A. L. Kharlanov, and J. A. McAllister, Nature (London) **394**, 157 (1998).
[18] L. M. Rodriguez-Martinez and J. P. Attfield, Phys. Rev. B **54**, R15 622 (1996).
[19] A. C. Larson and R. B. von Dreele, General Structure Analysis System, Report No. LAUR086-748, 1990, Los Alamos National Laboratory, Los Alamos, NM 87545.
[20] The χ^2 values less than 1 for composition $x \geqslant 0.6$ are due to the relatively smaller size of these samples and the resultant counting statistics. The structural parameters derived from the refined positional coordinates, used in the data analysis, are not affected by the difference in the statistical estimate of the goodness of fit for these samples.
[21] H. Kobayashi, M. Nagata, R. Kanno, and Y. Kawamoto, Mater. Res. Bull. **29**, 1271 (1994).
[22] A. J. Millis, Phys. Rev. B **53**, 8434 (1996).
[23] J. L. García-Muñoz, J. Fontcuberta, M. Suaaidi, and X. Obradors, J. Phys.: Condens. Matter **8**, L787 (1996).
[24] C. Boekema and F. Van Der Woude, Int. J. Magn. **3**, 341 (1972).
[25] K. Asai, K. Fujiyoshi, N. Nishimori, Y. Satoh, Y. Kobayashi, and M. Mizoguchi, J. Phys. Soc. Jpn. **67**, 4218 (1998).